Design and research of magnetic field sensor based on grapefruit optical fiber filled with magnetic fluid*

WANG Mengye[1], JIN Wa[1,2]**, LIU Xuejing[3], SUN Wenjie[1], ZHANG Chenhui[1], and BI Weihong[1,2]**

1. College of Information Science and Engineering, Yanshan University, Qinhuangdao 066000, China
2. The Key Laboratory for Special Fiber and Fiber Sensor of Hebei Province, Qinhuangdao 066000, China
3. College of Optical-Electrical and Computer Engineering, University of Shanghai for Science and Technology, Shanghai 200093, China

A novel magnetic field sensor was proposed based on the grapefruit optical fiber with the magnetic fluid injected into the six air holes. The sensor utilizes the Mach-Zehnder interference (MZI). The light is transmitted through the single-mode fiber to the fusion splice point and is divided into two parts. When the light passes through the cladding air hole with magnetic fluid, it interferes with the core light, and the change of the interference light is related with the change of the magnetic field. The sensor cavity length is 6 cm. It can be obtained from the experimental results that the magnetic field sensitivity reaches up to 2.243 nm/Oe with the range from 0 to 2.28 Oe. The sensor has the advantages of easy fabrication, easy installation and low cost. The findings provide new ideas for the study of ocean wind electromagnetic fields.

Magnetic field sensors have impressive significance in many applications, such as industry, medicine, and energy[1]. They have practical value in many fields, which have also prompted the scientific community to start the research and development of various functions, such as Hall sensors, anisotropic magneto resistive sensors, fluxgate magnetometers, superconducting quantum interference devices, etc[2-5]. This is also useful for people's daily life, such as medical magnetic resonance imaging (MRI). At the same time, people pay more and more attention to the optical fiber's light weight, simple manufacturing, anti-electromagnetic interference and low influence of various factors. Therefore, optical fiber measurement of magnetic field has increasingly become a hot spot of research, and the optical fiber magnetic field sensor has gradually become the general direction of research[6].

Various types of optical fiber sensors have been manufactured by splicing a section of photonic crystal fiber (PCF) to single mode fibers (SMF) using a low-cost optical fiber fusion splicer[7-10]. WEI et al[11] presented and experimentally demonstrated an optical magnetic field sensor using a fiber Bragg grating (FBG) injected magnetic fluid and a Sagnac ring to measure magnetic field. The experimental results showed that the sensitivity of the sensor was 102 pm/mT. At the same time,

TIAN et al[12] reported a magnetic field sensor with two SMFs and magnetic fluid. The experimental results demonstrated that the magnetic field sensitivity was 24.4 pm/Oe. WANG et al[13] proposed and verified a cascade structure of PCF and FBG to measure the magnetic field. The magnetic field sensitivity of the PCF reached 924.63 pm/mT. ZHU et al[14] reported a fiber magnetic field sensor based on surface plasmon resonance (SPR), and the sensing unit was made by splicing a section of PCF between two multi-mode fibers (MMFs). The sensitivity of the sensor was 4.42 nm/mT.

In this paper, a novel magnetic field sensor by injecting the magnetic fluid into six air holes of the grapefruit optical fiber is proposed to achieve magnetic field sensing. We investigate and experimentally demonstrate a magnetic field sensor using a special fiber fusion splicing SMF structure. The length of the grapefruit optical fiber is 6 cm filled with magnetic fluid into the cladding air holes of it, which relates to SMF to induce the Mach-Zehnder interference (MZI). The experimental results show that by changing the applied magnetic field, the interference spectrum is shifted during the transmission process. By analyzing the relationship between the interference spectrum offset and the magnetic field, the sensitivity of the magnetic field is 2.243 nm/Oe. At the same time, with the development and construction of offshore

wind farms, the number of submarine cables has risen sharply. In addition to the impact of wind farm construction on the marine ecological environment, the electromagnetic radiation generated by the operation of offshore wind farms has also become an environmental issue worthy of attention[15]. At present, there are relatively few measurement studies on the law of magnetic field changes caused by ocean wind power, and the electronic magnetic field sensor is not suitable for long-term in-situ monitoring. Therefore, the research on the structure of optical fiber magnetic field sensors is expected to lay the research foundation for ocean wind electromagnetic field monitoring technology.

Common optical fiber magnetic field sensors are mainly based on the Faraday effect, magneto strictive materials, and magnetic fluid[16]. This experiment uses a fiber optic magnetic field sensor based on magnetic fluid. Magnetic fluid is a new type of material with a diameter of about 5 nm. It has both the magnetic properties of ferromagnetic materials and the fluidity of liquids. Under different magnetic field intensities, the arrangement of the magnetic fluid particles results in different refractive indexes. The magnetic fluid has a good dynamic response to small external magnetic field changes. Compared with the optical fiber magnetic field sensor based on the magneto strictive effect, the one based on the magnetic fluid has higher sensitivity[17].

This paper uses the principle of MZI and the characteristic that the refractive index of magnetic fluid can be coordinated with the magnetic field to achieve magnetic field sensing. The sensor head structure is composed of two sections of SMF fusion spliced with a section of grapefruit optical fiber. When the incident light passes through the first fusion splice point, as shown in Fig.1, the light will be divided into two paths, one of which is transmitted through the grapefruit-shaped fiber core in the form of fundamental mode, while the other part propagates through the cladding. The two beams of light are coupled at the second fusion splice point, forming MZI[18].

The transmission intensity of the MZI could be expressed as[19]

$$I(\lambda) = I_{core}(\lambda) + I_{air}(\lambda) + 2\sqrt{I_{core}I_{air}}\cos(\theta), \qquad (1)$$

where I_{core} and I_{air} are the transmission intensities of light transmitted through the suspended core and the pores of the grapefruit optical fiber, respectively, and θ is the phase difference between them. Eq.(1) is used to calculate the specific formula for filling the grapefruit-type optical fiber with magnetic fluid. This is also one of the basic principles of this paper.

The sensor structure is filled with magnetic fluid in the air hole, and the structure is placed in the measured magnetic field. The magnetic fluid is based on a commercial product of EMG 705. Under magnetic field of 0—200 Oe, the refractive index change of magnetic fluid is approximately 0.003[20]. When the light passes through the cladding filled with magnetic fluid, and the magnetic field is changed at this time, the refractive index of the magnetic fluid will change. Therefore, the principle of measuring the magnetic field in this article is that the light passing through the cladding is affected by the magnetic field.
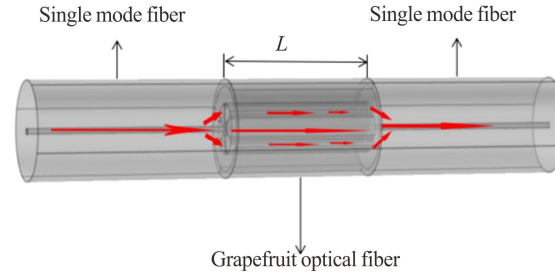

Fig.1 Experimental schematic of the proposed magnetic field sensor head structure

In order to study the free spectral range (*FSR*) of the grapefruit optical fiber, this paper adopts the finite element method to simulate the interference spectrum of the grapefruit optical fiber, and the effective refractive index of the fundamental mode is obtained by the simulation. Suppose the core diameter is *R*=6.6 μm, and the air hole length is *D*=30 μm. The distance between the air holes is *d*=21 μm, as shown in Fig.2.
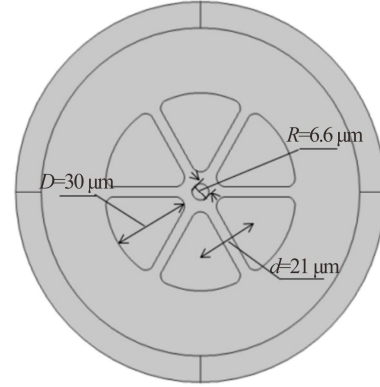

Fig.2 Grapefruit optical fiber model

The calculation formula of interference spectrum can be expressed as[21]

$$B(i, j) = 10 \cdot \lg\{0.2 + 0.2 +$$
$$2 \cdot \mathrm{sqrt}(0.2 \cdot 0.2) \cdot \cos\left[2\pi \cdot L \cdot \frac{N(i)}{M(j)}\right]\}, \quad (2)$$

where *B* is the interference result under different wavelengths, *L* is the sensor cavity length, and *N* is the effective refractive index difference. The magnetic fluid changes with the intensity of the external magnetic field, and the effective refractive index difference refers to the one between the fundamental mode of the fiber and the higher-order mode LP11. *M* is the wavelength range of the light source.

The finite element method is used to simulate and analyze the grapefruit fiber. In the case of 1 550 nm, the

refractive index of the fluid obtains the LP01 mode and LP11 mode of the grapefruit fiber by changing the magnetic field in the air hole, as shown in Fig.3, which displays the LP01 mode and LP11 mode and the difference between them.
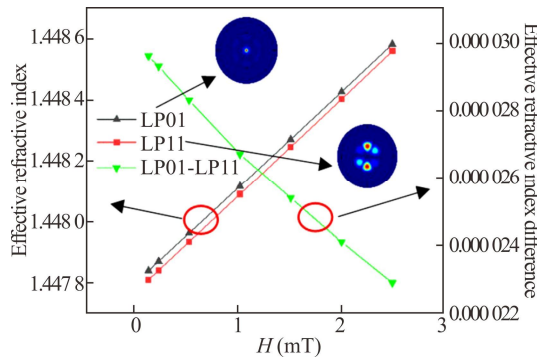

Fig.3 LP01 and LP11 modes of grapefruit fiber and the difference between effective refractive indexes of them

The interferogram obtained by analysis and calculation is shown in Fig.4(a). The program selects the light source range of 1 000—2 000 nm for calculation, and extracts the trough of the obtained interference pattern to obtain the trough map shown in Fig.4(b). The calculated sensitivity is 15 nm/Oe.
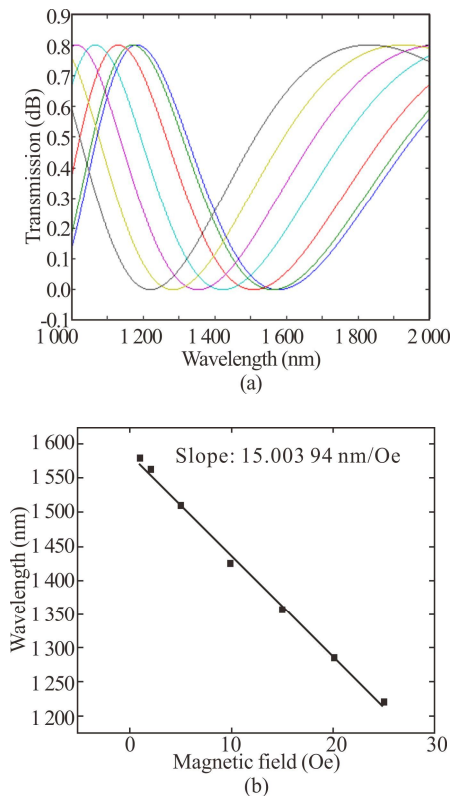

Fig.4 (a) Simulation interference map and (b) trough extraction map of the proposed magnetic field sensor
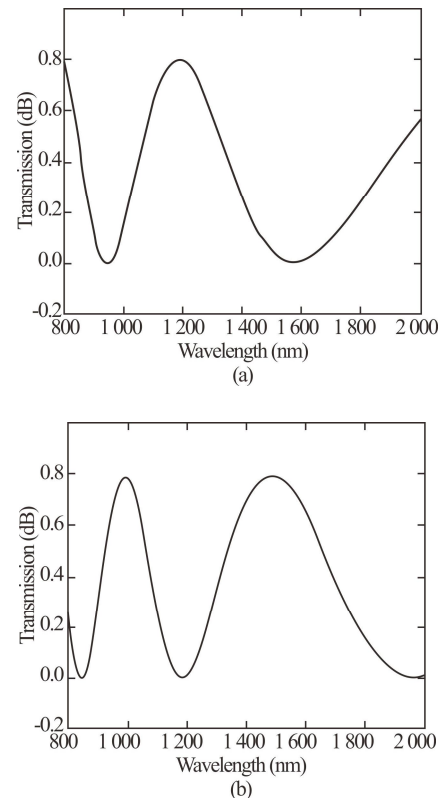
Through the comparison of different cavity lengths in Fig.5, it can be seen that the *FSR* obtained by simulation is gradually reduced. The formula for *FSR* is known as

$$FSR = \frac{\lambda_2 - \lambda_1}{\Delta n_{\text{eff}} L},\qquad(3)$$

where λ_1 and λ_2 are the wavelengths at two adjacent peaks in the interference pattern, Δn_{eff} is the effective refractive index difference, and L is the sensor cavity length. According to Eq.(3), the *FSR* gradually decreases with the increase of the cavity length, and the result obtained by the simulation is in accordance with the definition of *FSR*.

The experimental structure is set up, a broadband light source is selected as input light source, and the wavelength range is 1 520—1 610 nm. The optical signal processing system adopts the Yokogawa spectrometer produced in Japan, and its wavelength accuracy is nanometer, with wavelength resolution of 0.02 nm. The SMF is a 0.25 Corning single-mode bare fiber with a diameter of 125 μm, and the middle sensor part is a grapefruit optical fiber filled with magnetic fluid.

The production of the sensor head is shown in Fig.1. The cladding of the grapefruit optical fiber is peeled off, and the end face is cut to be flat and pasted on the glass slide. A thin needle tube is used to suck a small amount of magnetic fluid drop on one end of the optical fiber. It can be seen that due to the pressure, the magnetic fluid will be automatically attracted to the other end soon. The grapefruit optical fiber filled with the magnetic fluid is allowed to stand for one day and then spliced with the SMF at both ends. The structure of the end face under the electron microscope after splicing is shown in Fig.6.
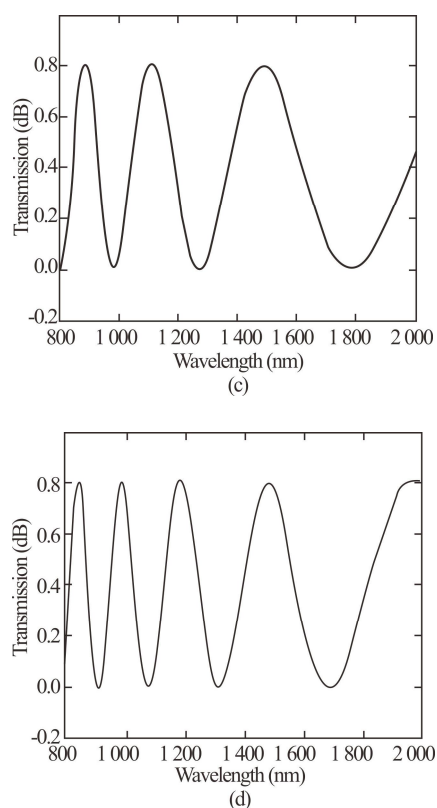
(c)

(d)

Fig.5 Simulated interferograms corresponding to different cavity lengths under the same magnetic field: (a) 8 cm; (b) 10 cm; (c) 15 cm; (d) 20 cm

Fig.6 Fiber splicing end face

The structure in this paper uses one end for fusion splicing, and the other end uses a ceramic sleeve with a diameter of 126 μm for cold splicing. Its diameter is slightly larger than that of the optical fiber. The cold splicing method makes the experiment more convenient and flexible.

The magnetic field monitoring in this paper refers to the monitoring of the quasi-static magnetic field under power frequency conditions. The magnetic field is produced by the current in the cable. The intensity of the magnetic field of a single-core cable is proportional to the size of the current[22]. A current source is used to generate a simulated magnetic field, and the current source is connected to a loop-wound coil barrel.

In order to shield the interference factors caused by the external magnetic field, a metal magnetic shielding cyl-

inder is used to cover the optical fiber sensor probe. The coil barrel in the shielding cylinder is used to generate the measured magnetic field. Put the sensor head into the coil barrel, and turn on the light source and the spectrometer. The variation of the spectrum on the spectrometer with the measured magnetic field is observed. The experimental structure is shown in Fig.7. The fluxgate magnetometer is used to measure the magnetic field. The fluxgate magnetometer probe is placed in the shielding cylinder. Adding a current source outside, since the shielding cylinder contains a coil of copper wire wound in the middle, a magnetic field will be generated inside the cylinder. The measured current and magnetic field intensity are shown in Tab.1.
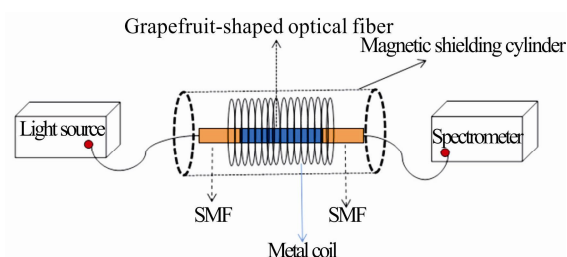

Fig.7 Experimental structure diagram

Tab.1 Current and magnetic field data

Current (A)	Magnetic field intensity (Oe)
0.10	0.225 63
0.11	0.248 44
0.12	0.270 92
0.13	0.294 34
0.14	0.317 05
0.15	0.339 62
0.16	0.362 11
0.20	0.453 96

The data in Tab.1 are processed to get a good linear relationship between current and magnetic field intensity, as shown in Fig.8.
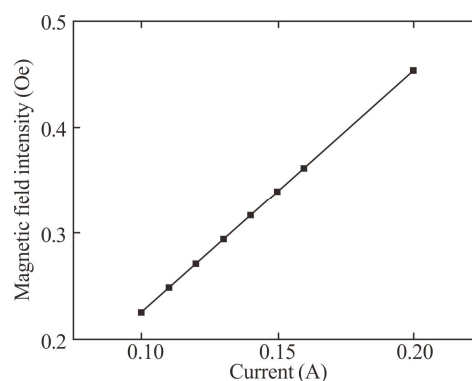

Fig.8 Relationship between current and magnetic field

The ratio *K* of the magnetic field intensity to the current calculated from Fig.8 is about 2.282 31, so the relationship between the simulated magnetic field intensity and the designed current is

$$B = 2.282\,31 * I. \tag{4}$$

In this experiment, the magnitude of the magnetic field in the range of 0—1 A is measured, and the magnitude of the magnetic field corresponding to the current in the range of 0—1 A in Tab.2 can be obtained by Eq.(4).

Tab.2 Magnetic field intensities corresponding to 0—1 A current

Current (A)	Magnetic field intensity (Oe)
0.10	0.22
0.15	0.34
0.20	0.45
0.25	0.57
0.30	0.68
0.35	0.79
0.40	0.91
0.45	1.02
0.50	1.14
1.00	2.28

In order to get the measurement accuracy of the sensor, this experiment will collect 10 groups of spectral data under different magnetic field intensities. The experimental structure is still constructed according to Fig.7. The sensor probe is placed in the middle of the metal coil of the external magnetic shielding cylinder, and the magnetic field is generated by energizing the metal coil. Note that we need to wait about 5 min to observe the phenomenon after applying a magnetic field. After the waveform is stable, you can observe the waveform of the fiber optic spectrometer to obtain the interference light spectra shown in Fig.9 under different magnetic field intensities. It can be clearly seen that the spectral curve has obvious drift with the increase of the magnetic field intensity. The relationship between peak wavelength drift and the measured magnetic field can be found.
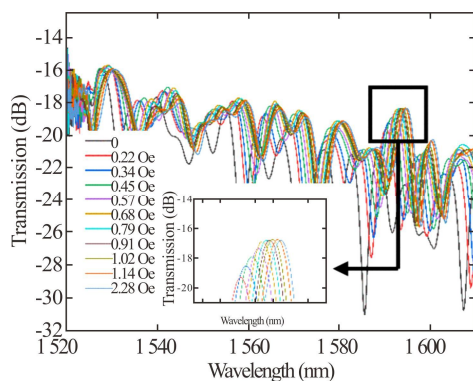

Fig.9 Corresponding interference patterns under different magnetic field intensities

Comparing the obtained experimental data with theoretical data, it can be seen that the *FSR* and theoretical results tend to be the same under different cavity lengths in Fig.10. As the cavity length gradually increases, the *FSR* gradually decreases. When the cavity length changes from 3 cm to 6 cm, its wave crests are obviously denser, which proves that the experimental results are consistent with the simulated ones.
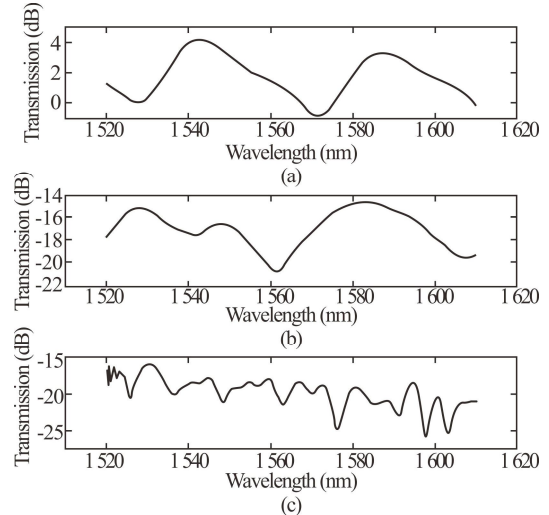

Fig.10 Measured interference patterns for different cavity lengths under the same magnetic field: (a) *L*=2 cm; (b) *L*=3 cm; (c) *L*=6 cm

It can be clearly seen that the interference pattern has a tendency to shift to the right as a whole in Fig.9. Here the 1 586—1 600 nm band is chosen. We can see from the changes in the intercepted part of the curve that the peak is shifted to the right in the magnetic field intensity range of 0—2.28 Oe. At the same time, we conduct the experiment in the magnetic field intensity range of 2.28—11.41 Oe. The experimental results are shown in Fig.11. The interference pattern shifts to the left. The experimental results are consistent with the blue shift results obtained by simulation. However, it is limited to the sensitivity range requirements of the initial production of the magnetic field sensor. Therefore, it is decided to select the results in the range of 0—2.28 Oe to calculate the sensitivity. The blue shift of the waveform in the latter part also further proves the consistency between the experiment and simulation.
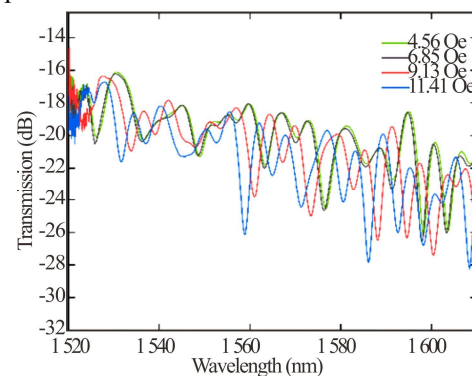

Fig.11 Corresponding interference patterns under magnetic field intensity in the range of 2.28—11.41 Oe

With the gradual increase of the magnetic field, the wave peaks regularly drift to the right. Therefore, the intensity of the magnetic field can be measured by analyzing the relationship between the wavelength shift and the change in the magnetic field.

The corresponding peaks of the waveform diagram under different magnetic fields can be found by analyzing and processing the obtained spectrogram in Tab.3. The sensitivity of the sensor designed in this experiment can be obtained by calculating the offset between the magnetic field change and the wavelength. The sensitivity calculation formula could be expressed as

$$P=\Delta\lambda/\Delta B, \tag{5}$$

where P is the sensitivity of the sensor, $\Delta\lambda$ is the offset of the wavelength, and ΔB is the change in the magnetic field. This article calculates the sensitivity of the sensor by calculating the average value of the sum of each two sets of experimental data, and the corresponding fitting curve is shown in Fig.12.

Tab.3 Wavelength peak values corresponding to magnetic field intensities

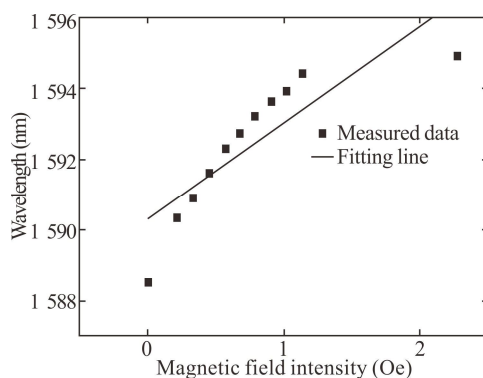| Magnetic field intensity (Oe)	Wavelength peak value (nm)
0	1 588.5
0.22	1 590.3
0.34	1 590.9
0.45	1 591.6
0.57	1 592.3
0.68	1 592.7
0.79	1 593.2
0.91	1 593.6
1.02	1 593.9
1.14	1 594.4
2.28	1 594.9

Fig.12 Fitting curve between wavelength and magnetic field intensity corresponding to the resonance peak transmission spectrum

Through calculation, ΔB=0.227 78 Oe, $\Delta\lambda$=0.511 nm, and P=2.243 nm/Oe can be obtained from Eq.(5). Due to the limited laboratory conditions, the intensity of the magnetic field can be increased and the related influence

experiments can be carried out to improve the sensitivity of the sensor.

At the same time, this experiment uses the same structure to fill alcohol and puts it in the temperature control box. The experimental results are shown in Fig.13. Under the normal condition, the spectra obtained at various temperatures are not regular. Therefore, the experimental results prove that this sensor is not sensitive to temperature.
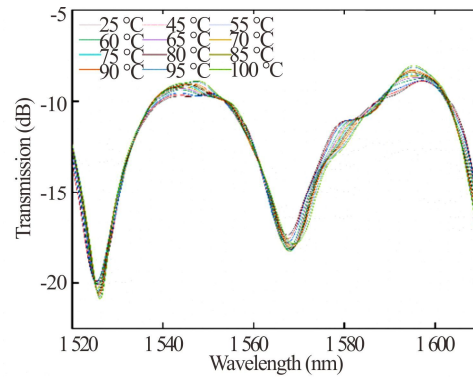

Fig.13 Temperature-sensitive experiment results

This paper proposes and manufactures an optical fiber magnetic field sensor based on the principle of MZI. After analysis, the *FSR* trend in experiment is consistent with the simulation. The magnetic fluid is filled in the grapefruit optical fiber air hole to make the magnetic fluid interact with the magnetic field. The refractive index of the magnetic fluid is affected by the magnetic field. The structure has a sensitivity of 2.243 nm/Oe. Both simulation and experiment prove that the method is feasible. At the same time, the experiment results prove that the sensor is not sensitive to temperature. Because of its simple structure, small footprint, and convenient operation, it is expected to be used for magnetic field measurement. After subsequent structural optimization, it is expected to contribute to the offshore wind power industry.

Statements and Declarations

The authors declare that there are no conflicts of interest related to this article.

References

[1] MUHAMMAD M B, BI W H, LIU X J, et al. Magnetic field sensor based on the magnetic fluid infiltrate-on into the cladding air holes of the solid-core photonic crystal fiber[J]. Optical engineering, 2019, 58(9)：096107.

[2] DANG H B, MALOOF A C, ROMALIS M V. Ultra-high sensitivity magnetic field and magnetization measurements with an atomic magnetometer[J]. Applied physics letters, 2010, 97(15)：151110.

[3] LANGFELDER G, TOCCHIO A. Operation of Lorentz-

force MEMS magnetometers with a frequency-offset between driving current and mechanical resonance[J]. IEEE transactions on magnetics, 2014, 50(1)：1-6.

[4]   SNOEIJ M F, SCHAFFER V, UDAYASHANKAR S, et al. Integrated fluxgate magnetometer for use in isolated current sensing[J]. IEEE journal of solid-state circuits, 2016, 51(7)：1684-1694.

[5]   RIPKA P, JANOSEK M. Advances in magnetic field sensors[J]. IEEE sensor journal, 2010, 10(6)：1108-1116.

[6]   CHEN Y F, HAN Q, LIU T G. All-fiber optical modulator based on no-core fiber and magnetic fluid as cladding[J]. Chinese physics B, 2015, 24(1)：014214.

[7]   WANG Y, YAN G F, LIAN Z G, et al. Liquid-level sensing based on a hollow core Bragg fiber[J]. Optics express, 2018, 26(17)：21656-21663.

[8]   JIN L, GUAN B O, WEI H F. Sensitivity characteristics of Fabry-Perot pressure sensors based on hollow-core microstructured fibers[J]. Journal of lightwave technology, 2013, 31(15)：2526-2532.

[9]   XIAO L M, JIN W, DEMOKAN M S, et al. Fabrication of selective injection microstructured optical fibers with a conventional fusion splicer[J]. Optics express, 2005, 13(22)：9014-9022.

[10] SALCEDA-DELGADO G, VAN NEWKIRK A, ANTONIO-LOPEZ J, et al. Compact fiber-optic curvature sensor based on super-mode interference in a seven-core fiber[J]. Optics letters, 2015, 40(7)：1468-1471.

[11] WEI F, LIU D, MALLIK A K, et al. Magnetic field sensor based on a tri-microfiber coupler ring in magnetic fluid and a fiber Bragg grating[J]. Sensors, 2019, 19(23)：5100.

[12] TIAN H, SONG Y X, LI Y Z, et al. Fiber-optic vector magnetic field sensor based on mode interference and magnetic fluid in a two-channel tapered structure[J]. IEEE photonics journal, 2019, 11 (6)：1-9.

[13] WANG J, PEI L, WANG J, et al. Magnetic field and temperature dual-parameter sensor based on magnetic fluid materials filled photonic crystal fiber[J]. Optics express, 2020, 28(2)：1456-1471.

[14] ZHU L, ZHAO N, LIN Q, et al. Optical fiber SPR magnetic field sensor based on photonic crystal fiber with the magnetic fluid as cladding[J]. Measurement science and technology, 2021, 32(7)：075106.

[15] ANDREW B G. Offshore renewable energy：ecological implications of generating electricity in the coastal zone[J]. Journal of applied ecology, 2005, 42(4)：605-615.

[16] CHEN F F, JIANG Y. Fiber optic magnetic field sensor based on the TbDyFe rod[J]. Measurement science and technology, 2014, 25(8)：085106.

[17] DAI M H, YANG X B, LI H L, et al. Magnetic field sensor based on magnetic fluid clad etched fiber Bragg grating[J]. Optical fiber technology, 2011, 17(3)：210213.

[18] DENG M, HUANG C, LIU D H, et al. All fiber magnetic field sensor with ferrofluid filled tapered microstructured optical fiber interferometer[J]. Optics express, 2015, 23(16)：20668-20674.

[19] SHI Q, CHEN D, JIANG X, et al. Refractive index sensor based on Mach-Zehnder interferometer formed by two cascaded single mode fiber corners[J]. Microwave and optical technology letters, 2014, 56(11)：2642-2645.

[20] CHEN Y F, YANG S Y, TSE W S, et al. Thermal effect on the field-dependent refractive index of the magnetic fluid film[J]. Applied physics letters, 2003, 82(20)：3481-3483.

[21] HUANG Y, WANG T Y, DENG C L, et al. A highly sensitive intensity-modulated optical fiber magnetic field sensor based on the magnetic fluid and multimode interference[J]. Journal of sensors, 2017, 2017：1-7.

[22] KIM J G, KIM S K, PARK M W, et al. Loss characteristic analysis of HTS DC power cable using LCC based DC transmission system[J]. IEEE transactions on applied superconductivity, 2012, 22(3)：5801304.